ACS Energy LETTERS

http://pubs.acs.org/journal/aelccp

Unveiling Solid Electrolyte Interphase Formation at the Molecular Level: Computational Insights into Bare Li-Metal Anode and $Li_6PS_{5-x}Se_xCl$ Argyrodite Solid Electrolyte

Andrey Golov and Javier Carrasco*

Cite This: *ACS Energy Lett.* 2023, 8, 4129–4135

Read Online

ACCESS | Metrics & More | Article Recommendations | Supporting Information

ABSTRACT: The development of high-energy-dense, sustainable all-solid-state batteries faces a major challenge in achieving compatibility between the anode and electrolyte. A promising solution lies in the use of highly ion-conductive solid electrolytes, such as those from the argyrodite family. Previous studies have shown that the ionic conductivity of the argyrodite Li_6PS_5Cl can be significantly enhanced by partially substituting S with Se. However, there remains a lack of fundamental knowledge regarding the effect of doping on the interfacial stability. In this study, we employ long-scale *ab initio* molecular dynamics simulations, which allowed us to gain unprecedented insights into the process of solid electrolyte interface (SEI) formation. The study focuses on the stage of nucleation of crystalline products, enabling us to investigate *in silico* the SEI formation process of Se-substituted Li_6PS_5Cl. Our results demonstrate that kinetic factors play a crucial role in this process. Importantly, we discovered that selective anionic substitution can accelerate the formation of a stable interface, thus potentially resolving anode−electrolyte compatibility issues.

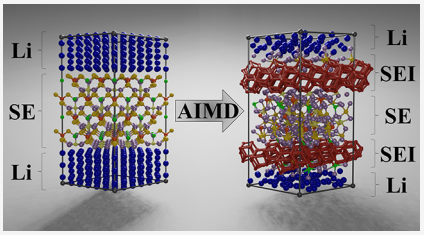

Electron and ion transfer at solid−solid interfaces plays a paramount role in the functioning of numerous devices that impact our daily lives. Controlling these processes is vital for multiple emerging technologies spanning a wide range of fields, including micro- and nanoelectronics,[1,2] renewable energy,[3,4] and 3D printing,[5−7] among others. Therefore, understanding solid−solid interfacial phenomena is crucial to advancing these critical areas of innovation.

In the context of battery research, the essential component that affects battery performance, safety, and the life cycle is the electrolyte−electrode interface. However, studying the formation and evolution of the so-called solid electrolyte interphase (SEI) presents significant challenges. These arise from the chemical and topological heterogeneity of the SEI as well as the nanoscale size of the interface region. Moreover, the SEI displays reactivity and complex dynamics that are difficult to assess experimentally due to the nonequilibrium state during battery operation. And the contribution of individual processes to the formation and evolution of interfaces can vary widely depending on several factors, such as cell chemistry, electrode/electrolyte combination, cycling protocol, and many more.[8−10]

Recent technological improvements in characterization tools offer new paths to a clearer understanding of the SEI and other interfacial phenomena.[11,12] Yet, to develop batteries with improved safety and efficiency for a wide variety of applications, multimodal and *operando* characterization techniques coupled with modeling and simulation approaches capable of identifying highly complex and interrelated processes are still required. In this regard, computational models based on *ab initio* calculations are becoming useful in predicting the stability and reactivity of solid electrolytes (SEs).[13−16] Such approaches hold significant promise in helping to advance our understanding of interfacial phenomena in batteries and other materials systems.

In this study, we utilize *ab initio* molecular dynamics (AIMD) simulations to provide insights into the early stage of the SEI layer formation process in all-solid-state batteries (ASSBs), where the SE is in contact with a Li-metal surface.

Received: July 7, 2023
Accepted: September 1, 2023
Published: September 13, 2023

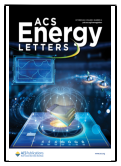

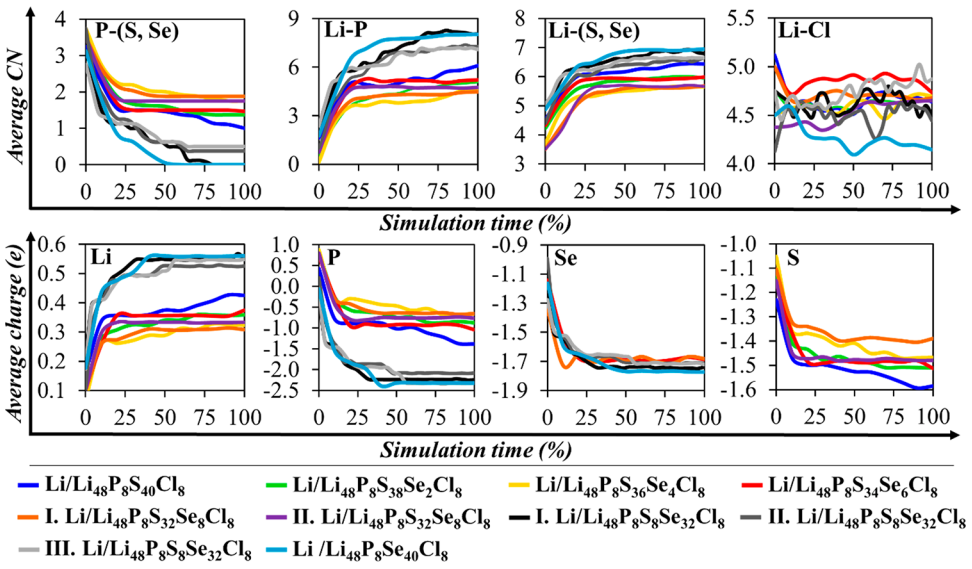

Figure 1. Evolution of the average coordination number and atomic charges of Li/$Li_6PS_{5-x}Se_xCl$ interface models (see Figure S2 for further details). Averaging was carried out over elements as well as over time with a time step of 10 ps. The considered P, S, and Se atoms belong to $PS_{4-x}Se_x^{3-}$ groups.

We focus on the Li-argyrodite SE family, which is promising for the development of ASSBs due to its exceptional room-temperature Li-ion conductivities and low cost.[17−20] AIMD simulations have previously helped identify decomposition products and reaction mechanisms at the interface between Li_6PS_5Cl and model Li metal surfaces,[21−23] but a further understanding of SEI growth and evolution is still desired. To address this challenge, we focus specifically on the Li/$Li_6PS_{5-x}Se_xCl$ interface systems, where we hypothesize that Se should accelerate interfacial reactivity and enable the time and length scales accessible by AIMD to examine SEI formation and growth. We also considered interfaces with F-doped argyrodite, which previously showed good cyclability with the Li metal anode.[24] Furthermore, to comprehensively analyze SEI evolution in such complex interfaces, we implemented a novel algorithm that exhaustively tracks crystal growth as a structure-assembling process from building units represented by natural tiles.

To construct the Li/$Li_6PS_{5-x}Se_xCl_{1-y}F_y$ (where x = 0, 0.25, 0.5, 0.75, 1, 4, 5 and y = 0, 0.125) interface models, we first explored the configuration space of the bulk SE. Detailed information about the structural models and density functional theory (DFT) calculations is given in the Supporting Information. Results of the calculations show that Se substitution within the argyrodite structures yields an increase in the binding energy (Figure S1). Conversely, F doping has the opposite effect. Like in the case of pure Li_6PS_5Cl, we also find that the cubic Se-substituted phases are metastable.[25−27] Thus, any symmetry break caused by the thermal fluctuation of atoms or the introduction of substituting atoms may trigger a transition to triclinic phases. In fact, our calculations reveal that out of the 449 initially cubic structures, the geometry relaxation of 118 cases resulted in this phase transition. During the structure reorganization, Li ions undergo displacement from 24g to 48h sites, and there is a shift observed in the positions of halogen ions from the centers of intraframework cages. The energy difference between the cubic and triclinic phases is around 60 meV/atom. Consequently, for the purpose of our study, we exclusively focused on the triclinic structure.

For a given composition, the arrangement of Se atoms within the structure has no significant impact on the binding energy of the system. The energy gap between the lowest and highest energy configurations does not exceed 12 meV/atom. Overall, there is no evident correlation between the occupancy of Se ions in the 4c and 16e sites and the energy of the structure, as depicted in Figure S1. Consequently, a straightforward synthesis of the $Li_6PS_{5-x}Se_xCl_{1-y}F_y$ structure from Li_2S, P_2S_5, Se, and LiCl(F) should result in a relatively even distribution of Se ions between the 4c and 16e sites. This finding is consistent with experimental data for the $Li_6PS_{5-x}Se_xI$ structure.[28]

We utilized the obtained $Li_6PS_{5-x}Se_xCl_{1-y}F_y$ bulk structures to construct 15 interface Li/$Li_6PS_{5-x}Se_xCl_{1-y}F_y$ models (Figure S2), which were subsequently subjected to AIMD simulations (see the Supporting Information for complete details). Our results indicate that when in contact with Li metal, the argyrodite SEs are reduced. Specifically, this leads to the decomposition of $PS_{4-x}Se_x^{3-}$ groups, as reflected by a decrease in the computed P−S and P−Se coordination numbers (CNs) and a systematic increase in Li−S and Li−Se CNs (Figure 1 and Figure S3 top). The change in the local atomic environment is accompanied by electron transfer from the Li metal to the P, S, and Se atoms of the $PS_{4-x}Se_x^{3-}$ groups (Figure 1 and Figure S3 bottom). Overall, the reaction proceeds by the stepwise breaking of P−S and P−Se bonds until the complete reduction of $PS_{4-x}Se_x^{3-}$ groups to P^{3-}, S^{2-}, and Se^{2-} anions. These findings are consistent with previous computational[21,24,27] and experimental[29] studies of the Li/Li_6PS_5Cl interface.

At low concentrations of Se and F, there is no apparent relationship between the reaction rate and the amount of substituted elements (Figure 2). Additionally, the type of Se-substituted sites (4c and 16e) does not appear to affect the rate of SE degradation. However, substituting most of the S atoms with Se atoms accelerates the reaction. This is evident in the (I) Li/$Li_{48}P_8S_8Se_{32}Cl_8$, (II) Li/$Li_{48}P_8S_8Se_{32}Cl_8$, (III) Li/$Li_{48}P_8S_8Se_{32}Cl_8$, and Li/$Li_{48}P_8Se_{40}Cl$ interface models, which exhibit the highest reaction rates. In these models, the SEs

https://doi.org/10.1021/acsenergylett.3c01363
ACS Energy Lett. 2023, 8, 4129−4135

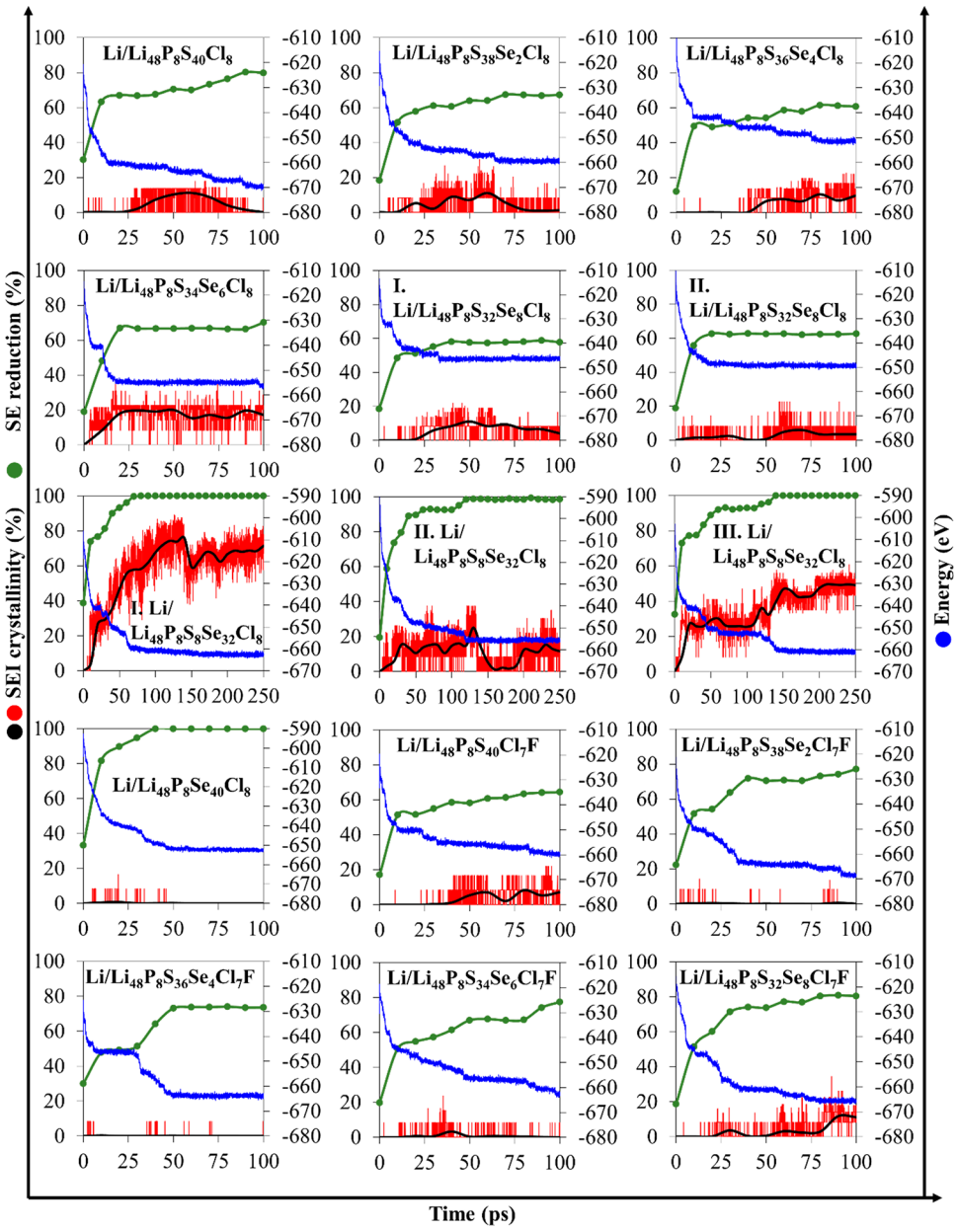

Figure 2. Evolution of potential energy, percentage of reduced SE, and SEI crystallinity for different Li/$Li_6PS_{5-x}Se_xCl_{1-y}F_y$ interface models. The black curve indicates the average over 10 ps of time step crystallinity of the SEI.

undergo near or complete reduction within the first 80, 120, 70, and 40 ps of simulation, respectively (Figure 2). The high reaction rate of these models makes them ideal for studying *in silico* the kinetics of the solid-state reaction and the underlying mechanism of SEI formation.

From a thermodynamic point of view, the reaction between Li metal and $Li_6PS_{5-x}Se_xCl_{1-y}F_y$ should lead to the formation of several compounds, including LiCl, LiF, Li_3P, Li_2S, and Li_2Se. The reaction can be described by the equation:

$$Li_6PS_{5-x}Se_xCl_{1-y}F_y + 8Li = (1-y)LiCl + yLiF + Li_3P + (5-x)Li_2S + xLi_2Se \quad (1)$$

Although a sufficiently long AIMD simulation could potentially show the formation of these crystalline phases, the required simulation time may not be achievable in the framework of DFT-based calculations. Nevertheless, for the interface models exhibiting a high reaction rate, we may expect the appearance of small crystalline regions (crystalline seeds) within the amorphous products. To identify such regions along the AIMD trajectory, we employed the concept of natural tilings.[30,31] Within this approach, structures of expected products are divided into cage-like atomic configurations, so-called tiles, forming periodic space-filling tessellation (Figure 3). Compared to individual atoms or coordination figures, tiles provide a more comprehensive representation of structural features. Although different structures may have the same tiles, the overall tile set and the way they are assembled are unique for each structure type. These properties make natural tiling a valuable tool for the prediction of the possible structure of a final product based on the analysis of atomic configurations of intermediate products at the initial stages of the reaction. In other words, we can guess the possible structure of the SEI by

https://doi.org/10.1021/acsenergylett.3c01363
ACS Energy Lett. 2023, 8, 4129−4135

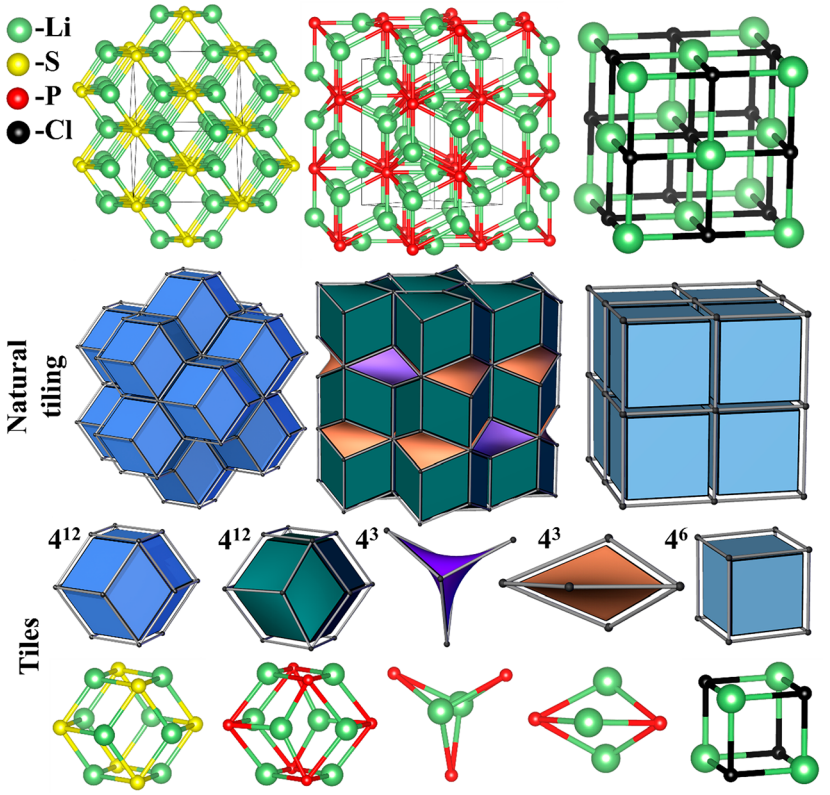

Figure 3. Structures of Li_2S, Li_3P, and LiCl (top), their natural tilings (middle), tiles, and the corresponding structural cages (bottom).

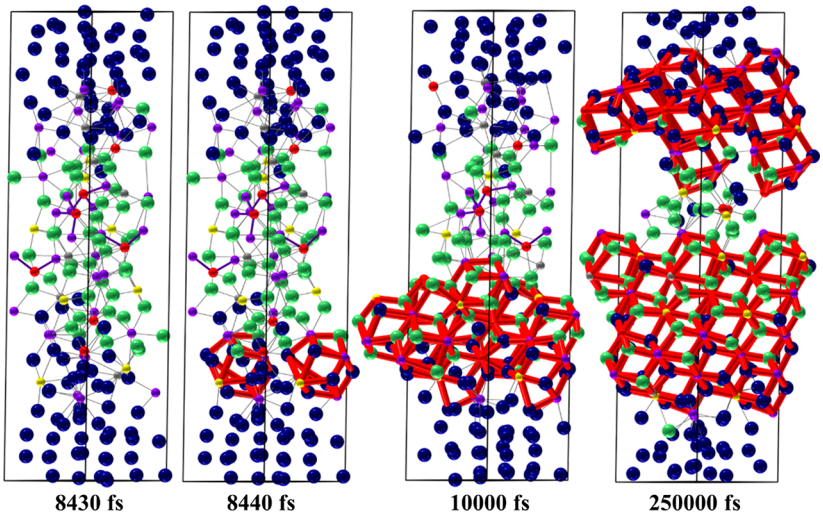

Figure 4. Structural evolution of the SEI observed through four consecutive snapshots extracted from the AIMD trajectory for the (I) Li/$Li_{48}P_8S_8Se_{32}Cl_8$ interface model. The crystalline regions are depicted by red rhombic dodecahedra. Li metal, Li of electrolyte, S, Se, P, and Cl are depicted by blue, green, yellow, purple, red, and gray spheres, respectively.

analyzing the frequency occurrence of tiles of expected products and the way they are assembled along the AIMD trajectory. For instance, the natural tilings of Li_2S and LiCl are a rhombic dodecahedron and cubic honeycomb, respectively. The Li_3P has a structure topologically similar to that of the Li_2S, with additional tiles located between layers of the hexagonal-packed rhombic dodecahedron (Figure 3). Natural tilings of Li_2Se and LiF are identical to those of Li_2S and LiCl, respectively, as they share the same antifluorite and rock salt structure types. In total, these structures have three topologically unique tiles ($[4^{12}]$, $[4^3]$, and $[4^6]$) and seven inequivalent cages Li_8S_6, Li_8Se_6, Li_8P_6, Li_2P_3, Li_3P_2, Li_4Cl_4, and Li_4F_4 which correspond to these tiles. The presence of these cages within the AIMD frames is proxies of crystalline phase nucleation.

Interestingly, although the analysis of AIMD trajectories did not reveal the presence of the previously mentioned cages set, Li_8An_6 (where An = P, S, Se, Cl) was found to occur frequently. These rhombic dodecahedron cages contain not only sulfur and selenium, but also phosphorus, and chalcogenide ions. These intricate structures interconnect through their faces, giving rise to the distinctive pattern of a

https://doi.org/10.1021/acsenergylett.3c01363
ACS Energy Lett. 2023, 8, 4129−4135

rhombic dodecahedron. This defining arrangement becomes most prominently evident in the final frame of the AIMD simulation, as depicted in Figure 4 for the (I) Li/$Li_{48}P_8S_8Se_{32}Cl_8$ interface model and further elaborated in Figure S4 for other interfacial models. Thus, we can conclude that the SEI structure should correspond to the LiCl(F)−Li_3P−Li_2S−Li_2Se solid solution, which has the antifluorite structure type. The overall reaction can be described by the equation

$$Li_6PS_{5-x}Se_xCl_{1-y}F_y + 8Li = Li_{14}PS_{5-x}Se_xCl_{1-y}F_y \quad (2)$$

Our analysis also reveals that Li_2An_3, Li_3An_2, and Li_4An_4 cages are predominantly found in the amorphous interface region. Unlike the rhombic dodecahedra, they connect chaotically via edges and vertices, thereby failing to form high-ordered structures. Therefore, the presence of these cages cannot be used as evidence of Li_3P and LiCl phase nucleation.

These findings offer a new perspective on the Li/argyrodite interface structure, which is contrary to previous theoretical and experimental works. A prior *in situ* X-ray photoelectron spectroscopy (XPS) study of interphase growth on Li metal electrodes revealed degradation of the Li_6PS_5Cl SE over time. Specifically, the peaks corresponding to PS_4^{3-} groups, S 2p, and P 2p XPS spectra decreased, while peaks attributed to S^{2-} and P^{3-} increased.[29] Based on these data, it was inferred that the reaction resulted in the formation of Li_2S, Li_3P, and LiCl. Although XPS can offer insights into the composition and the local atomic environment of a compound, it cannot directly determine the crystal structure on its own. This can lead to ambiguity in the identification of structures with identical compositions and oxidation states of elements. While DFT calculations can aid in finding the lowest energy products by enumerating all possible variants,[23] this approach may overlook kinetic considerations. Conversely, AIMD simulations can provide access to kinetic aspects, yet such insight is often only limited to unveiling intermediate reaction products within a reasonable simulation time.[21,24,27]

To move beyond these limitations, we found that considering tiles as a unit of growth allows for observing the onset of the nucleation process *in silico* (Figure 4). For example, in the initial 8 ps of the AIMD simulation for the (I) Li/$Li_{48}P_8S_8Se_{32}Cl_8$ interface model, the reduction of the SE reached approximately 76% (Figure 2). As the reaction front progresses from the interface toward the bulk of the SE, rhombic dodecahedral cages begin to emerge near the Li-metal slab. These atomic clusters act as nucleation sites, growing by attaching new cages to the faces of existing ones. Within approximately 10 ps of the simulation, a 9 Å thick, 2-periodic layer of the crystalline product is formed. The formation of this crystalline layer is accompanied by a slowdown in the reaction rate, evident from the decreasing slope of the SE reduction curve over time (Figure 2). A second drop in the reaction rate is observed at around 50 ps, likely due to the formation of a coating layer on the opposite side of the SE slab. Although the coating layer is not thick enough to completely prevent electron transfer from the Li metal to the SE, the reaction proceeds until the SE is fully reduced. At the final AIMD frame, the interface model consists of an unreacted Li metal slab and two crystalline layers of reduced electrolyte with a thin amorphous region in between (as shown in Figure 4 and Figure S4). The formation of an ideal crystalline layer is impeded by the different crystallographic orientations of crystalline products on opposite sides of the Li metal slab. By 250 ps of the simulation, the crystallinity of the SEI reaches 71.5%. This value is determined by evaluating the ratio between the number of atoms within the crystal nuclei and the overall amount of product, as described in eq 2.

It is important to note that across all the examined interface models noticeable fluctuations in crystallinity occur over time (Figure 2). These variations stem from the inherently stochastic nature of the nucleation process, which is governed by a myriad of factors.[32] Chief among these are the intricate interplay of local environmental conditions and thermal fluctuations, both of which can induce substantial transformations in the dimensions, morphology, and composition of the crystal nuclei as time unfolds. The spontaneously formed crystal nuclei can either continue to grow or become amorphous. For example, in the case of (I) Li/$Li_{48}P_8S_8Se_{32}Cl_8$, (III) Li/$Li_{48}P_8S_8Se_{32}Cl_8$, Li/$Li_{48}P_8S_{36}Se_4Cl_8$, and Li/$Li_{48}P_8S_{34}Se_6Cl_8$ models, there is a trend of progressively increasing crystallinity. However, for the Li/$Li_{48}P_8S_{40}Cl_8$, Li/$Li_{48}P_8S_{38}Se_2Cl_8$, and (I) Li/$Li_{48}P_8S_{32}Se_8Cl_8$ models, the nuclei stop growing at around 50 ps without reaching the critical size, with further reversion to an amorphous state. The Li/$Li_{48}P_8S_{40}Cl_8$, Li/$Li_{48}P_8S_{38}Se_2Cl_7F$, and Li/$Li_{48}P_8S_{36}Se_4Cl_7F$ models exhibit significantly fewer nucleation events. The nuclei appearing almost immediately became amorphous, leading to low crystallinity. The remaining models show chaotic changes in crystallinity over the simulation time. Interestingly, a high reaction rate does not always correspond to a high rate of crystallization. For example, electrolytes Li_6PSSe_4Cl and Li_6PSe_5Cl both exhibited high reaction rates, but only the first one formed a high-ordered SEI structure. Therefore, directed Se substitution of 16e sites of the SE can aid in the rapid formation of a passivation layer, protecting against further electrolyte degradation.

According to the DFT calculation of the $Li_{14}PS_{5-x}Se_xCl_{1-y}F_y$ modeled structure (Table S2), the formation of individual LiCl, LiF, Li_3P, Li_2S, and Li_2Se phases is more energetically favorable than the corresponding solid solution. However, the energy difference between these products is not significant. Both reactions have identical stoichiometry and follow the same redox mechanism. The only disparity between these reactions lies in the structure of their products, which exhibit different coordination numbers of Li−P, Li−Cl, and Li−F atoms. Overall, the energy change of the interface models is primarily associated with the reduction of the SE by Li metal, rather than the subsequent structural reorganization. Indeed, we found that the percentage of reduced SE is linearly correlated with the potential energy (Figure S5). Furthermore, regardless of any changes in SEI crystallinity, the energy remains almost constant when the electrolyte reduction reaches a plateau (Figure 2). Thus, in this case, the main driving force that determines the reaction path is kinetic factors. Specifically, the formation of $Li_{14}PS_{5-x}Se_xCl_{1-y}F_y$ solid solution or amorphous products is expected to have an activation barrier lower than that of individual lithium salts (LiCl, LiF, Li_2S, Li_2Se, and Li_3P). The solid solution crystallizes with minimal spatial ion redistribution, while crystallization of several phases requires ion diffusion from the reduced SE to the forming phases.

Overall, this study provides valuable insights into the reaction mechanisms and nucleation processes at the Li/$Li_6PS_{5-x}Se_xCl_{1-y}F_y$ interface. The understanding of these processes is crucial for designing SEs with improved stability and performance in ASSBs. It has been shown that the

https://doi.org/10.1021/acsenergylett.3c01363
ACS Energy Lett. 2023, 8, 4129−4135

formation of the LiCl(F)−Li_3P−Li_2S(Se) solid solution or amorphous products at the interface is driven by kinetic factors, as they have lower activation barriers compared to the individual lithium salts. The incorporation of Se atoms into the 16e sites of the argyrodite structure accelerates the reaction kinetics and promotes the nucleation of a highly ordered SEI layer capable of protecting the SE against further degradation. Furthermore, the introduced approach, harnessing natural tiling to dissect AIMD simulations, establishes a valuable framework that holds promise for future investigations delving into nucleation processes occurring in solutions or at interfaces. This framework is particularly relevant to studies centered on SEI and cathode−electrolyte interphase formation. Implementing these developed analysis techniques and algorithms in future works can provide deeper insights into the formation and behavior of such complex interfaces, facilitating complementary experimental characterizations, and driving the advancement of more efficient and reliable energy storage devices.

■ ASSOCIATED CONTENT

Supporting Information

The Supporting Information is available free of charge at https://pubs.acs.org/doi/10.1021/acsenergylett.3c01363.

Additional characteristics of the interface models and computational details (PDF)

■ AUTHOR INFORMATION

Corresponding Author

Javier Carrasco − *Centre for Cooperative Research on Alternative Energies (CIC energiGUNE), Basque Research and Technology Alliance (BRTA), 01510 Vitoria-Gasteiz, Spain; IKERBASQUE, Basque Foundation for Science, 48009 Bilbao, Spain;* orcid.org/0000-0003-3117-6933; Email: jcarrasco@cicenergigune.com

Author

Andrey Golov − *Centre for Cooperative Research on Alternative Energies (CIC energiGUNE), Basque Research and Technology Alliance (BRTA), 01510 Vitoria-Gasteiz, Spain*

Complete contact information is available at: https://pubs.acs.org/10.1021/acsenergylett.3c01363

Notes

The authors declare no competing financial interest.

■ ACKNOWLEDGMENTS

This work was supported by the European Commission through the H2020 program under Grant agreement number 875028 (SUBLIME Project). We gratefully acknowledge the technical support provided by the Barcelona Supercomputing Center and the computer resources from University of Zaragoza and SCAYLE (QHS-2022-1-0001, QHS-2022-2-0001, QHS-2023-1-0005), SGI/IZO-SGIker UPV/EHU, and i2BASQUE academic network.

■ REFERENCES

(1) Hacker, C. A.; Bruce, R. C.; Pookpanratana, S. Interface Engineering for Nanoelectronics. *ECS Trans* **2017**, *80* (1), 119−131.

(2) Sun, Z.; Bai, Y.; Liu, J.; Jian, G.; Guo, C.; Zhang, L.; Pu, Y. Interface Engineering in Ferroelectrics: From Films to Bulks. *J. Alloys Compd.* **2022**, *909*, 164735.

(3) Wang, M.; Feng, Z. Interfacial Processes in Electrochemical Energy Systems. *Chem. Commun.* **2021**, *57* (81), 10453−10468.

(4) Chen, P.; Tong, Y.; Wu, C.; Xie, Y. Surface/Interfacial Engineering of Inorganic Low-Dimensional Electrode Materials for Electrocatalysis. *Acc. Chem. Res.* **2018**, *51* (11), 2857−2866.

(5) Ponnada, S.; Babu Gorle, D.; Chandra Bose, R. S.; Sadat Kiai, M.; Devi, M.; Venkateswara Raju, C.; Baydogan, N.; Kar Nanda, K.; Marken, F.; Sharma, R. K. Current Insight into 3D Printing in Solid-State Lithium-Ion Batteries: A Perspective. *Batter Supercaps* **2022**, *5* (8), No. e202200223.

(6) McOwen, D. W.; Xu, S.; Gong, Y.; Wen, Y.; Godbey, G. L.; Gritton, J. E.; Hamann, T. R.; Dai, J.; Hitz, G. T.; Hu, L.; Wachsman, E. D. 3D-Printing Electrolytes for Solid-State Batteries. *Adv. Mater.* **2018**, *30* (18), 1707132.

(7) Hunde, B. R.; Woldeyohannes, A. D. 3D Printing and Solar Cell Fabrication Methods: A Review of Challenges, Opportunities, and Future Prospects. *Results in Optics* **2023**, *11*, 100385.

(8) Kraytsberg, A.; Ein-Eli, Y. Recent Developments in the Field of Sulfide Ceramic Solid-State Electrolytes. *Energy Technology* **2023**, *11*, 2201291.

(9) Heiskanen, S. K.; Kim, J.; Lucht, B. L. Generation and Evolution of the Solid Electrolyte Interphase of Lithium-Ion Batteries. *Joule* **2019**, *3* (10), 2322−2333.

(10) Meda, U. S.; Lal, L.; Sushantha, M.; Garg, P. Solid Electrolyte Interphase (SEI), a Boon or a Bane for Lithium Batteries: A Review on the Recent Advances. *J. Energy Storage* **2022**, *47*, 103564.

(11) Atkins, D.; Ayerbe, E.; Benayad, A.; Capone, F. G.; Capria, E.; Castelli, I. E.; Cekic-Laskovic, I.; Ciria, R.; Dudy, L.; Edström, K.; Johnson, M. R.; Li, H.; Lastra, J. M. G.; De Souza, M. L.; Meunier, V.; Morcrette, M.; Reichert, H.; Simon, P.; Rueff, J.; Sottmann, J.; Wenzel, W.; Grimaud, A. Understanding Battery Interfaces by Combined Characterization and Simulation Approaches: Challenges and Perspectives. *Adv. Energy Mater.* **2022**, *12* (17), 2102687.

(12) Adenusi, H.; Chass, G. A.; Passerini, S.; Tian, K. V.; Chen, G. Lithium Batteries and the Solid Electrolyte Interphase (SEI)—Progress and Outlook. *Adv. Energy Mater.* **2023**, *13* (10), 2203307.

(13) Xiao, Y.; Wang, Y.; Bo, S.-H.; Kim, J. C.; Miara, L. J.; Ceder, G. Understanding Interface Stability in Solid-State Batteries. *Nat. Rev. Mater.* **2020**, *5* (2), 105−126.

(14) Xiao, Z.; Yuan, R.; Zhao, T.; Kuang, Y.; Yin, B.; Liu, C.; Song, L. Advances and Applications of Computational Simulations in the Inhibition of Lithium Dendrite Growth. *Ionics (Kiel)* **2023**, *29* (3), 879−893.

(15) Wu, Y.-T.; Tsai, P.-C. Ab Initio Interfacial Chemical Stability of Argyrodite Sulfide Electrolytes and Layered-Structure Cathodes in Solid-State Lithium Batteries. *JOM* **2022**, *74* (12), 4664−4671.

(16) Wang, A.; Kadam, S.; Li, H.; Shi, S.; Qi, Y. Review on Modeling of the Anode Solid Electrolyte Interphase (SEI) for Lithium-Ion Batteries. *NPJ. Comput. Mater.* **2018**, *4* (1), 15.

(17) Arnold, W.; Buchberger, D. A.; Li, Y.; Sunkara, M.; Druffel, T.; Wang, H. Halide Doping Effect on Solvent-Synthesized Lithium Argyrodites Li_6PS_5X (X= Cl, Br, I) Superionic Conductors. *J. Power Sources* **2020**, *464*, 228158.

(18) Deiseroth, H.-J.; Kong, S.-T.; Eckert, H.; Vannahme, J.; Reiner, C.; Zaiß, T.; Schlosser, M. Li_6PS_5X: A Class of Crystalline Li-Rich Solids With an Unusually High Li^+ Mobility. *Angew. Chem., Int. Ed.* **2008**, *47* (4), 755−758.

(19) Ruhl, J.; Riegger, L. M.; Ghidiu, M.; Zeier, W. G. Impact of Solvent Treatment of the Superionic Argyrodite Li_6PS_5Cl on Solid-State Battery Performance. *Advanced Energy and Sustainability Research* **2021**, *2* (2), 2000077.

(20) Yamagishi, Y.; Morita, H.; Nomura, Y.; Igaki, E. Visualizing Lithium Distribution and Degradation of Composite Electrodes in Sulfide-Based All-Solid-State Batteries Using Operando Time-of-Flight Secondary Ion Mass Spectrometry. *ACS Appl. Mater. Interfaces* **2021**, *13* (1), 580−586.

(21) Cheng, T.; Merinov, B. V.; Morozov, S.; Goddard, W. A. Quantum Mechanics Reactive Dynamics Study of Solid Li-Electrode/Li_6PS_5Cl-Electrolyte Interface. *ACS Energy Lett.* **2017**, *2* (6), 1454−1459.
(22) Camacho-Forero, L. E.; Balbuena, P. B. Exploring Interfacial Stability of Solid-State Electrolytes at the Lithium-Metal Anode Surface. *J. Power Sources* **2018**, *396*, 782−790.
(23) Wang, C.; Aoyagi, K.; Aykol, M.; Mueller, T. Ionic Conduction through Reaction Products at the Electrolyte−Electrode Interface in All-Solid-State Li^+ Batteries. *ACS Appl. Mater. Interfaces* **2020**, *12* (49), 55510−55519.
(24) Arnold, W.; Shreyas, V.; Li, Y.; Koralalage, M. K.; Jasinski, J. B.; Thapa, A.; Sumanasekera, G.; Ngo, A. T.; Narayanan, B.; Wang, H. Synthesis of Fluorine-Doped Lithium Argyrodite Solid Electrolytes for Solid-State Lithium Metal Batteries. *ACS Appl. Mater. Interfaces* **2022**, *14* (9), 11483−11492.
(25) Wang, Z.; Shao, G. Theoretical Design of Solid Electrolytes with Superb Ionic Conductivity: Alloying Effect on Li^+ Transportation in Cubic Li_6PA_5X Chalcogenides. *J. Mater. Chem. A* **2017**, *5* (41), 21846−21857.
(26) D'Amore, M.; Daga, L. E.; Rocca, R.; Sgroi, M. F.; Marana, N. L.; Casassa, S. M.; Maschio, L.; Ferrari, A. M. From Symmetry Breaking in the Bulk to Phase Transitions at the Surface: A Quantum-Mechanical Exploration of Li_6PS_5Cl Argyrodite Superionic Conductor. *Phys. Chem. Chem. Phys.* **2022**, *24* (37), 22978−22986.
(27) Golov, A.; Carrasco, J. Molecular-Level Insight into the Interfacial Reactivity and Ionic Conductivity of a Li-Argyrodite Li_6PS_5Cl Solid Electrolyte at Bare and Coated Li-Metal Anodes. *ACS Appl. Mater. Interfaces* **2021**, *13* (36), 43734−43745.
(28) Schlem, R.; Ghidiu, M.; Culver, S. P.; Hansen, A.-L.; Zeier, W. G. Changing the Static and Dynamic Lattice Effects for the Improvement of the Ionic Transport Properties within the Argyrodite $Li_6PS_{5-x}Se_xI$. *ACS Appl. Energy Mater.* **2020**, *3* (1), 9−18.
(29) Wenzel, S.; Sedlmaier, S. J.; Dietrich, C.; Zeier, W. G.; Janek, J. Interfacial Reactivity and Interphase Growth of Argyrodite Solid Electrolytes at Lithium Metal Electrodes. *Solid State Ion* **2018**, *318*, 102−112.
(30) Blatov, V. A.; Delgado-Friedrichs, O.; O'Keeffe, M.; Proserpio, D. M. Three-Periodic Nets and Tilings: Natural Tilings for Nets. *Acta Crystallogr., Sect. A* **2007**, *63* (5), 418−425.
(31) Anderson, M. W.; Gebbie-Rayet, J. T.; Hill, A. R.; Farida, N.; Attfield, M. P.; Cubillas, P.; Blatov, V. A.; Proserpio, D. M.; Akporiaye, D.; Arstad, B.; Gale, J. D. Predicting Crystal Growth via a Unified Kinetic Three-Dimensional Partition Model. *Nature* **2017**, *544* (7651), 456−459.
(32) Karthika, S.; Radhakrishnan, T. K.; Kalaichelvi, P. A Review of Classical and Nonclassical Nucleation Theories. *Cryst. Growth Des* **2016**, *16* (11), 6663−6681.

https://doi.org/10.1021/acsenergylett.3c01363
ACS Energy Lett. 2023, 8, 4129−4135